RAÚL FAINCHTEIN

SCANNING TUNNELING MICROSCOPY OF ORGANIC CONDUCTORS AND SUPERCONDUCTORS

The scanning tunneling microscope has been successfully applied to investigate the surface structures of organic conductors and superconductors and the molecular arrangements in these solids that make their electrical conductivity behave as if the materials were one-dimensional.

INTRODUCTION

The scanning tunneling microscope (STM) developed ten years ago by Binning et al.[1] has emerged as a powerful tool for investigating the electronic and structural properties of surfaces. By using an extremely sensitive distance-dependent electrical current sensor, namely, the tunneling current between the sample and probing tip, the STM can image the electronic density distribution of a material at the surface with atomic resolution. Since its development, the instrument has been very effective in providing real space images of crystalline surfaces and in revealing unknown details of the surface structure. The great dynamic range of the STM scan enables it to resolve features that range in dimension from atomic sizes to micrometer sizes, without direct contact or apparent surface modification. The versatility of the technique allows instruments to operate in air, ultrahigh vacuum, and liquid environments at high and low temperatures. The technique has been successfully applied to a variety of problems in the fields of surface science,[1] superconductivity,[2] charge density waves,[3] atomic surface modification,[4] and recently to electrical switching by a single atom.[5] In this article, the STM is used as a tool to study the structure and the electron density of states of organic conductors and superconductors, the effects of low dimensionality in the electron density of states, and the consequences of the structure to the electrical conductivity of these materials.

Interest in the study of organic materials as potential candidates for high-temperature superconductivity was motivated by Little[6] in 1964 when he proposed that an arrangement of one-dimensional organic chains in a polarizable medium was a promising candidate for high-temperature superconductivity. Little predicted that the large polarization could be provided by side chains surrounding the conducting chains, which would induce (via polarization excitations) a great effective attraction between electrons in the conducting chains, leading to pairing (a necessary condition for superconductivity) at high temperatures.

7,7,8,8-Tetracyanoquinodimethane (TCNQ)-based salts were believed to offer structural similarities to the model proposed by Little and, therefore, the potential realization for high-temperature superconductivity in an organic material. Tetrathiofulvalene-7,7,8,8-tetracyano-quinodimethane (TTF-TCNQ), synthesized, among others, by Dwaine O. Cowan and coworkers at The Johns Hopkins University in 1972, offered the highest room-temperature electrical conductivity ($500~\Omega^{-1} \cdot cm^{-1}$) of any known organic compound at the time. TTF-TCNQ, however, does not make the transition to a superconducting state. Although the electrical resistivity decreases as the material is cooled, it reaches a minimum at ≈ 59 K, below which the resistivity increases until the material finally becomes an insulator.

The transition from a metallic to an insulating state in TTF-TCNQ is the consequence of a prediction in 1954 by Peierls.[7] Peierls[7] and Fröhlich[8] showed that a one-dimensional free-electron gas (a model in which the conduction electrons in a material are presumed to be free particles in a one-dimensional box) displays an inherent instability to the interaction of a potential having a wave number equal to $2 k_F$ (where k_F is the Fermi wave number, the quantum mechanical momentum of the highest occupied electron energy level in the material). Such instability was shown to produce a large amplitude modulation in the charge density coupled to a lattice distortion. This effect gives rise to a collective state of the electrons in the system called a charge density wave (CDW) that opens a gap in the electron density of states (the number of electronic levels available to the electrons at a particular energy per unit volume and unit energy) at the Fermi level and sometimes produces a metal–insulator transition. (See the boxed insert for a discussion of charge density waves.) The phenomenon occurs below a certain transition temperature T_P, known as the Peierls transition. (At temperatures above T_P, the combination of atomic vibrations and elastic restoring forces in the material destroys the CDW.)

Although several organic superconductors have been synthesized, Little's prediction has been undermined by the effects of electron instabilities in the structural and transport properties of low-dimensional systems. The first organic material known to become a superconductor was tetramethyltetraselenafulvalene-hexafluorophosphate, $(TMTSF)_2PF_6$, discovered in 1979.[9] $(TMTSF)_2PF_6$

CHARGE DENSITY WAVES

   The normal state of electrical conduction in a low-dimensional metallic system is susceptible to electron density instabilities. Such instabilities can, in some cases, cause a metal–insulator transition. The driving force of this phenomenon is a divergence in the generalized static electronic susceptibility (the electron response function) of the material as a result of a perturbation in the electronic potential with a wave vector equal to $2k_F$, where k_F is the Fermi wave number. The perturbation can be established by electron–phonon interactions (which result in charge density waves [CDW's]) or electron-spin interactions (which result in spin density waves).

   The energy dispersion relation (the energy E versus momentum k) of a free-electron one-dimensional metal, such as the one shown in illustration A, is given by $E = k^2/2m$ until the momentum approaches a reciprocal lattice point π/a, where a gap created by the periodicity of the lattice opens up. In a classical picture, as shown in illustration B, the atoms are represented by open circles that are equally spaced by a lattice parameter a, where core electrons are drawn as filled circles on top of the atoms, and free delocalized electrons are depicted by the continuous electron density line $\rho(r)$. The electrons of the system occupy energy levels according to the Pauli exclusion principle from the bottom of the energy band up to the Fermi energy E_F.

   When the free-electron one-dimensional metal is perturbed by a potential with wave vector $\mathbf{q}$, the electron response function $\chi(q)$ increases as the frequency approaches $2k_F$, and at $q = 2k_F$ it diverges. This perturbation opens a gap at the Fermi energy of the system as seen in the energy dispersion relation of illustration C, and the free electron density of the system $\rho(r)$ develops an oscillating component with a period equal to $2a$, as shown in illustration D.

   For a comprehensive review on CDW's, the reader is referred to a 1988 article by Grüner.[47]

   is a quasi-one-dimensional material that requires high pressure (superconducting transition temperature $T_c = 0.9$ K at $P = 12$ kbar) to suppress the metal–insulator transition created by a spin density wave (a CDW analog based on electron spin interactions). Since the discovery of superconductivity in organic materials, the synthesis of new superconducting organic structures has been directed toward materials that display higher dimensionality to avoid the metal–insulator transition predicted by Peierls and Fröhlich.

   Until the recent discovery of superconductivity in the doped (C_{60}) fullerenes, progress in the race to increase the superconducting transition temperature in organic materials has been motivated by the discovery of the superconducting properties of the κ-phased di[bis(ethylenedithiolo)tetrathiafulvalene] (BEDT-TTF) (or ET for short) layered compounds. Since the synthesis in 1990 of κ-di[bis(ethylenedithiolo)tetrathiafulvalene]copper-(I)bis(isothiocyanate), κ-$[(ET)_2]^+[Cu(NCS)_2]^-$,[10] which exhibits a $T_c = 10.4$ K in DC resistance measurements, a
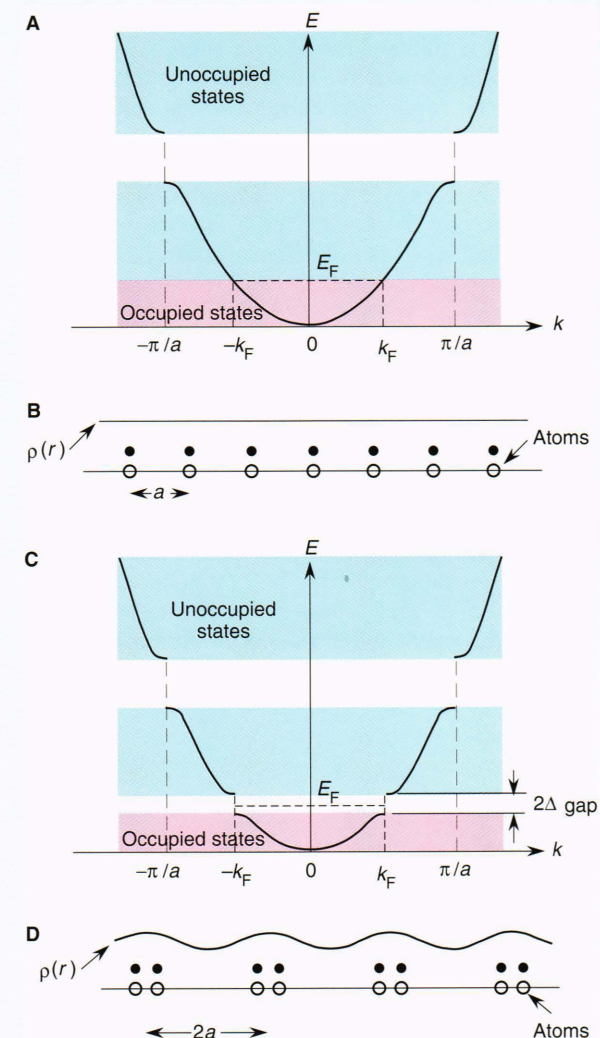
new series of κ-phased compounds have been synthesized with T_c's in excess of 11 K.[11] These layered materials offer striking similarities (strong coupling and short coherence lengths) in their superconducting behavior to the high-T_c superconducting ceramics.

SCANNING TUNNELING MICROSCOPY

   The STM can produce images of the local electron density of states near the Fermi energy at the scanning tip. The tunneling current between a material and a sharp tip is proportional to the local electron density of states of the material near the Fermi energy.[12,13] By scanning the tip above the surface while maintaining the tunneling current constant, the instrument maps a surface of constant tunneling probability that is affected by the electron density of states and the surface structure. Images of the surface topography with atomic resolution and the presence of a CDW can be resolved with the STM. The instrument can also provide spectroscopic information on the density of states near the Fermi energy.

The technique is based on the quantum mechanical phenomenon of electrons tunneling through a nonconducting gap at the application of a small potential bias (Fig. 1A). When an electrical potential is applied between two electrodes, a potential barrier like the one shown in Figure 1A is formed. Electrons tunnel through the potential barrier from occupied to unoccupied states in the direction dictated by the applied potential. The tunneling current between two infinite parallel electrodes separated by a nonconducting gap of distance d can be simplified for low voltages and small gaps to the following expression:

$$I \approx \frac{V}{d} \exp(-A\bar{\phi}^{1/2}d) , \qquad (1)$$

where $A = 1.025$ (eV)$^{-1/2}$ Å^{-1}, $\bar{\phi}$ is the average potential barrier height between the two electrodes, and V is the bias potential between the electrodes. This relationship between current and separation distance indicates that for a tunneling barrier approximately 4 eV high, a change of 1 Å in the separation distance will bring about a change of one order of magnitude in the tunneling current. Therefore, by maintaining a constant current through a feedback mechanism, electronic structures of the surface can be topographically mapped (Fig. 1B).
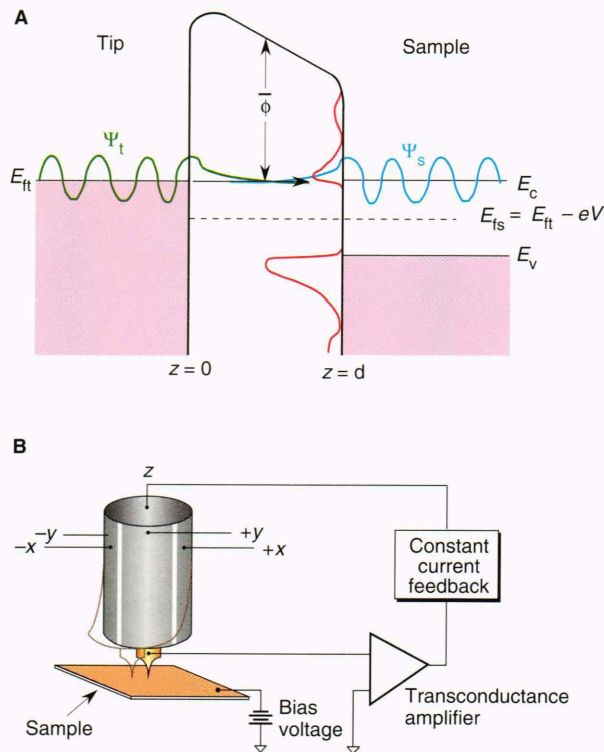
A rigorous description of the tunneling current is more complicated. It involves a quantum mechanical description of the three-dimensional tunneling case and can be calculated using first-order perturbation theory. In this approach, the tunneling current is given by the following expression:[14]

$$I = \frac{2\pi e}{\hbar} \sum_{\mu\nu} f(E_\mu)[1 - f(E_\nu + eV)]|M_{\mu\nu}|^2 \, \delta(E_\mu - E_\nu) \qquad (2)$$

where $\hbar = h/2\pi$, h is Plank's constant, e is the electron charge, $M_{\mu\nu}$ is the tunneling matrix element (representing the probability of electrons tunneling from tip to sample), $f(E)$ is the Fermi occupational probability distribution function of the electrons in the tip or the sample as a function of energy E, V is the bias voltage across the tunneling barrier, and E_μ and E_ν represent the energies of states μ or ν, where μ and ν run over all possible states of the tip and the sample, respectively. The tunneling matrix element $M_{\mu\nu}$ can be written using the transfer Hamiltonian formalism developed by J. Bardeen[15] in 1961 as

$$M_{\mu\nu} = \frac{\hbar^2}{2m} \int dS \cdot \left(\Psi_\mu^* \nabla \Psi_\nu - \Psi_\nu \nabla \Psi_\mu^* \right) , \qquad (3)$$

where Ψ represents the quantum mechanical wave function, and the integral is over any plane in the barrier region. Equations 2 and 3 are in principle all that are needed to calculate the tunneling current. In practice, however, this is very difficult, and some approximations are necessary. By assuming that both sides of the tunneling barrier (tip and sample) are two independent and weakly coupled systems that interact via the tunneling barrier (which is treated as the perturbing Hamiltonian), the tunneling current can be represented as a convolution of the electron density of states $\rho(E)$ of the two electrodes weighted by their appropriate Fermi statistical occupation distribution $f(E)$.[16]

$$I \approx \int_{-\infty}^{\infty} \rho_s(E + eV)\rho_t(E) \, |M(E)|^2 \\ \times [f(E) - f(E - eV)] \, dE , \qquad (4)$$

where the subindices s and t refer to the sample and tip, respectively. When one electrode is configured as a sharp tip with only a few atoms, or ideally one atom, at the end, the wave function of the electrons at the tip can be considered localized. With this assumption, the dependence of the current on the electron density of states of the tip becomes a constant, and, therefore, the tunneling current can be expressed as

$$I \approx \int_0^{eV} \rho(E)D(E,V)dE , \qquad (5)$$

where $\rho(E)$ is the sample surface density of states and $D(E, V)$ is the transmission coefficient of the tunneling barrier at a voltage V. This indicates that by maintaining

Figure 1. Schematic representation of the operational principles that drive a scanning tunneling microscope. **A.** Energy E versus distance z of a tunneling junction, where E_f is the Fermi level, E_v is the top of the valence, band E_c is the bottom of the conduction band, Ψ is the electron wave function, and ϕ is the tunneling barrier height. The subscripts t and s refer to tip and sample. The red curves depict the electron density of states of the sample. **B.** Schematic representation of a scanning tunneling microscope. The segmented tube is a piezoelectric ceramic that scans and tracks by applying voltages in the different segments.

334

a constant current, the STM maps a region of constant electron density up to an energy eV from the Fermi level, multiplied by the tunneling transmission coefficient.

When analyzing the current dependence on the separation distance (Eq. 1), it is easy to understand why the instrument is able to image the electronic topography by scanning the tip over the sample while maintaining a constant current (Fig. 1B). Another very important feature of the STM is the ability to provide electronic spectroscopic information of the sample surface (Eq. 5) because of its highly localized electronic probe. This feature is particularly important in determining local parameters, such as the effective barrier heights between surfaces, and I versus V conductance curves and their derivatives. By oscillating while ramping the bias voltage of the tunneling junction, the normalized conductance with respect to the bias voltage can be measured. This measurement provides direct information regarding the electron density of states of the probed surface. As one may suspect, problems may arise when the conditions of low bias voltage cannot be maintained, because of a lack of states in the specimen to tunnel to or from, such as with insulators.

ORGANIC CONDUCTORS

TTF-TCNQ is a compound made of planar TTF and TCNQ molecules that undergo a charge transfer when combined. In the solid phase, similar ions stack on top of one another to form columns (Fig. 2). The direction along the column is tilted with respect to the normal to the plane of the molecules that constitute the column. The proximity of the molecules along the stacks provides a strong overlap of their electronic orbitals. The charge transfer that occurs upon formation produces half-filled bands within the stacks. As a result of these structural arrangements, most of the properties of these materials are highly anisotropic, including their electrical conductivity, which is metallic only in one direction, that is, the direction parallel to the stacks. The electron mean free path (average distance between scatterers) is larger than the intermolecular spacing along the direction of the stacks and shorter than the intermolecular spacing in directions perpendicular to the stacks; these materials have been designated quasi-one-dimensional conductors.

Single crystals of TTF-TCNQ are typically prepared by a thermal diffusion method in a solution of acetonitrile in an H-shaped diffusion tube, as described by Kaplan.[17] The needle-shaped crystals have typical dimensions of 1 to 3 mm by 0.2 to 0.5 mm by 0.01 to 0.1 mm. The monoclinic crystal structure is shown in Figure 2, where reported parameters are $a = 12.298$ Å, $b = 3.819$ Å, $c = 18.468$ Å, and $\beta = 104.46°$.[18] The temperature dependence of the DC electrical resistivity[19] is shown in Figure 3. The resistivity of TTF-TCNQ decreases with temperature, until at 53 K the material undergoes a metal–insulator transition.

TTF-TCNQ was the first organic material imaged with an STM[20] (see Fig. 4 for the highest-resolution STM image of this material reported to date, which was made at APL) and is only one example of charge transfer organic salts where the molecules arrange themselves in columnar stacks. It is possible to make chemical substitutions in the constituent molecules of these materials. The salts made with these substitutions provide different geometric arrangements of the stacks in the solids they form. Thus, the degree of cross talk between the stacks that form the crystal can be controlled, going from a system with almost noninteracting chains, such as tetramethyltetrathio-fulvalene-7,7,8,8-tetracyanoquinodimethane (TMTTF-TCNQ), the tetramethyl derivative of TTF-TCNQ (CH_3 radicals substituting the hydrogen at the extreme of the TTF molecule; see Fig. 2), to tetramethyltetraselenaful-
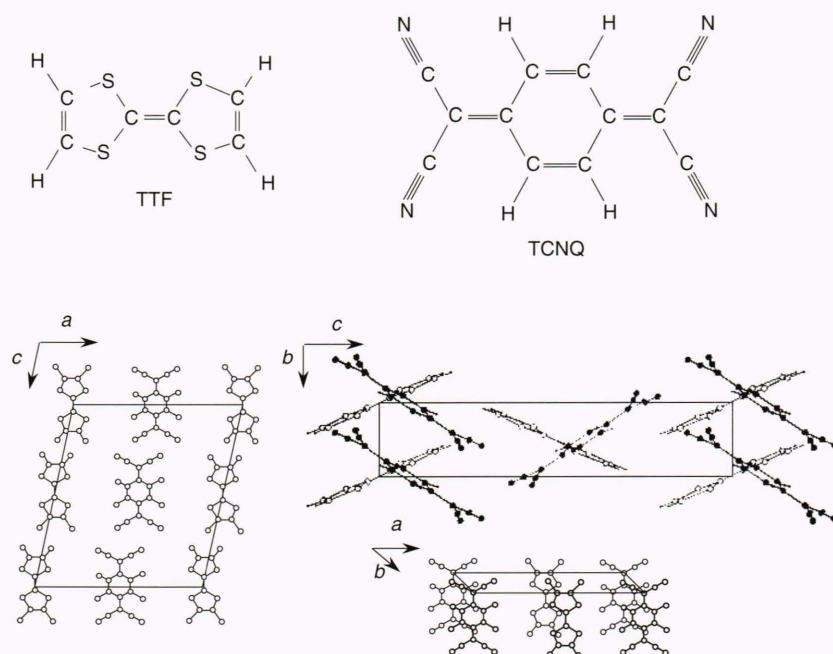

Figure 2. Molecular structure of TTF and TCNQ and schematic representation of the structure of TTF-TCNQ along different crystallographic planes.
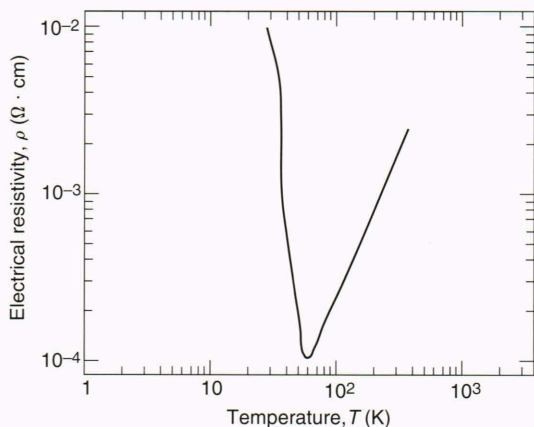
Figure 3. Electrical resistivity of TTF-TCNQ as a function of temperature. Reprinted, with permission, from Ref. 19, p. 359.

valene-7,7,8,8-tetracyanoquinodimethane (TMTSF-TCNQ), a system with a higher degree of chain coupling by the substitution of the sulfur atoms by selenium atoms in the TMTTF molecule. (An STM image of the surface of TMTTF-TCNQ is shown on the inside back cover of the Vol. 12, No. 3, July–September 1991 issue of the *Johns Hopkins APL Technical Digest.*)

Ambient room temperature STM measurements were made with a commercial instrument from Digital Instruments. The crystals were mounted on gold films evaporated on cleaved mica substrates at 200°C and fixed to the substrates with conductive silver paint. The STM can be operated in the constant current mode (using feedback response that is fast compared with the scanning speed and recording the piezoelectric deflections), as well as in the constant height mode (using feedback response that is slow compared with the scanning speed and recording the tunneling current fluctuations). Both modes of operation revealed the same structural features in the images. The tunneling current was set at values less than or equal to 2 nA; 1 nA was used for most images. The scans were made with positive and negative bias voltages in the range of −1 to 1 V. On all conductive samples, changes in the bias voltage within the specified range produced

no apparent change in the structures revealed by the images. Increasing the bias voltage while maintaining the same preset constant current level (and thus increasing the junction resistance) in either polarity, however, caused a decrease in image resolution in some instances. Line scanning rates of 156 Hz were used when operating in the constant current mode, and rates of 4 Hz were used when operating in the constant height mode. Images measuring 200 by 200 pixels or 400 by 400 pixels were obtained. No manipulations other than background plane subtraction were applied to the images. Platinum with 20% iridium tips were used. The tips were either mechanically (at Digital Instruments) or electrochemically sharpened.[21] Better results were obtained with electrochemically sharpened tips. All the images presented are direct photographs of the computer screen.

The low-temperature images and current–voltage (I–V) tunneling characteristics of the tip–sample junction were obtained with a home-built ultrahigh vacuum (UHV) low-temperature STM in collaboration with Shuheng Pan and Alex L. de Lozanne at The University of Texas at Austin. This STM has a base pressure of 10^{-11} torr and a variable temperature range from 10 to 400 K. The sample temperature is continuously controlled and monitored. The samples used for low-temperature STM studies were mounted on copper substrates using silver paint. Tips and samples can be transferred in and out of the chamber without breaking the vacuum through a load lock and can be ion-milled and annealed *in situ.*

Figure 5 presents two images of the *ab* plane of TTF-TCNQ taken in UHV over a 120 Å by 120 Å area. Figure 5A was taken at room temperature, whereas Figure 5B was taken at 78 K. In all the STM images presented, the color scale is used to represent variations in the direction perpendicular to the surface. Figures 5A and 5B were taken with the STM operated in constant current mode, meaning that height variations of the image represent the vertical position that the tip holds on top of the surface to maintain a constant tunneling current. Therefore, light points represent positions of the scan where the STM tip moved away from the surface to maintain a constant tunneling current. Dark points represent positions where the STM tip moved closer to the surface to keep the

Figure 4. Pseudo-three-dimensional projection of a 35 Å by 35 Å scanning tunneling microscope image of the *ab* plane of TTF-TCNQ ($V_{tip} = -10$ mV, $I_{tun} = 2$ nA, constant current mode). Under the image are schematic representations of portions of the molecular structures to help identify different elements of the image.
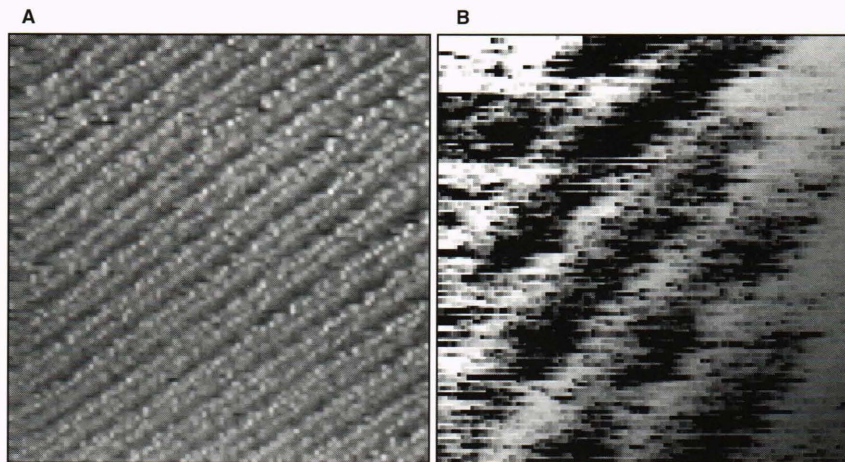
A **B**
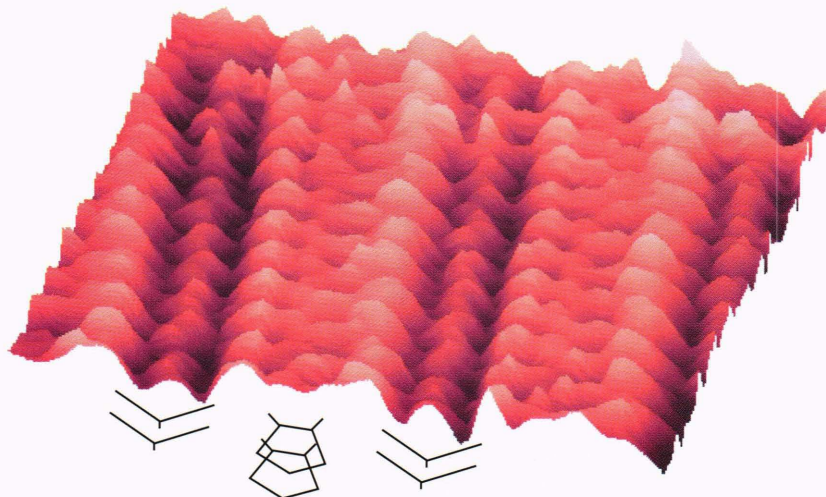
Figure 5. 120 Å by 120 Å scanning tunneling microscope images of the *ab* plane of TTF-TCNQ in an ultra-high vacuum. **A.** At room temperature (V_{tip} = −50 mV, I_{tun} = 0.2 nA, constant current mode). **B.** At 78 K (V_{tip} = −50 mV, I_{tun} = 1 nA, constant current mode).

tunneling current at the same constant value. Figure 5A reveals the existence of diagonal parallel rows that extend throughout the sample. Between double peak rows, an alternate row parallel to the others but of reverse contrast is observed. The distance between similar features in the direction perpendicular to the rows is 12 Å, corresponding to the *a* lattice parameter. Molecular identification in high-resolution scans (Fig. 4) is aided by comparing the images with plots of regions of constant electron density of states calculated by molecular orbital simulations (MOS).[18] Projections of the MOS on the *ab* plane helped to identify the double rows in Figure 4 with the CN radicals at the extreme of the TCNQ molecules (see the *ab* plane of Fig. 1); the high electron density regions of the TTF molecule lie farther down in the *ab* plane and therefore appear as dark rows. As the temperature drops, an additional modulation appears that is parallel to the room temperature structural rows. This superstructure is the most prominent feature in the image at 78 K. The spacing between similar features in the direction perpendicular to the rows is 24 Å, which corresponds to a $2a$ spacing.

Until recently, the presence of a CDW in TTF-TCNQ and in other low-dimensional systems has been known from diffraction studies.[22–26] For TTF-TCNQ, a $4k_F$ CDW superstructure commensurate with the lattice is known to exist at temperatures below 38 K with a $4a$ by $3.4b$ by c modulation period. An abrupt increase of the modulation frequency in the a direction from a $4a$ period to a $2a$ period is known to occur as the temperature is raised near and above 51 K.[27] This superstructure has been associated with a $2k_F$ CDW.[28]

The STM reveals in real space the superstructure in the electron density of states created by the CDW modulation. In the STM observations of TTF-TCNQ, the presence of a CDW becomes apparent at temperatures of 80 K. A $2a$ modulation starts to form at 80 K and completely dominates the appearance of the images at 78 K; the accompanying CDW modulation in the b direction was not resolved by the STM images. Attempts to image the material below 54 K failed. Simultaneous electrical conductivity measurements along the b direction showed a substantial drop, and at ≈39 K, the material became a small-gap semiconductor.

The results of tunneling spectroscopy on the *ab* plane of TTF-TCNQ are presented in Figure 6. The I–V characteristics reveal metallic behavior until a temperature of 11 K is reached. Then a flat region in the center of the I–V curve develops that indicates the opening of a gap in the electron density of states near the Fermi level. As previously stated, the normalized tunneling conductance is proportional to the electron density of states.

Reproducible I–V characteristics were obtained by pressing the tip onto the sample. A gap in the electron density of states begins to develop at 38 K and is fully formed for temperatures below 11 K. The opening of an energy gap $E_g = 2\Delta$ (where Δ is the activation energy of the excitation) in the electron density of states corresponding to $2\Delta_{CDW} \approx 100$ mV is measured. This value, although consistent with other point-contact tunneling measurements,[29] is roughly twice the gap value obtained from the DC conductivity measurements.[30]

ORGANIC SUPERCONDUCTORS

The organic superconductor κ-[(ET)$_2$]$^+$[Cu(NCS)$_2$]$^-$ was first synthesized by Urayama et al.[10] in 1988. X-ray studies of κ-[(ET)$_2$]$^+$[Cu(NCS)$_2$]$^-$ revealed a structure formed by the interstacking of planes of standing ET molecules that pair themselves to form dimers in a two-dimensional network arrangement, together with planes formed by Cu(NCS)$_2$ polymer chains located between the ET planes[31] (Fig. 7). Although the structure of the material has been known for some time, uncertainty remains as to the existence of some kind of disorder and an additional lattice modulation in certain crystals visible through X-ray diffraction that has been attributed to the presence of a stacking fault (a half-anion chain displacement in the c direction at every $4b$ unit cell displacement).[10,31,32]

Single crystal samples of κ-[(ET)$_2$]$^+$[Cu(NCS)$_2$]$^-$ were prepared by Samuel T. D'Arcangelis, a graduate student in Cowan's group at The Johns Hopkins University, using standard electrochemical methods. The experimental details have been reported elsewhere.[33] The crystals have a flake-like appearance with straight edges. They range in area from 0.5 mm by 0.5 mm to 2 mm by 2 mm with an approximate thickness of 0.1 mm. The crystal structure is monoclinic, as depicted in Figure 7. The structural parameters of the material for two different temperatures

Figure 6. Tunneling spectroscopy of the *ab* plane of TTF-TCNQ in ultrahigh vacuum with $Pt_{80}Ir_{20}$ counterelectrode tips. Tunneling current I and tunneling conductance dI/dV versus tip bias voltage V are plotted for four different temperatures.
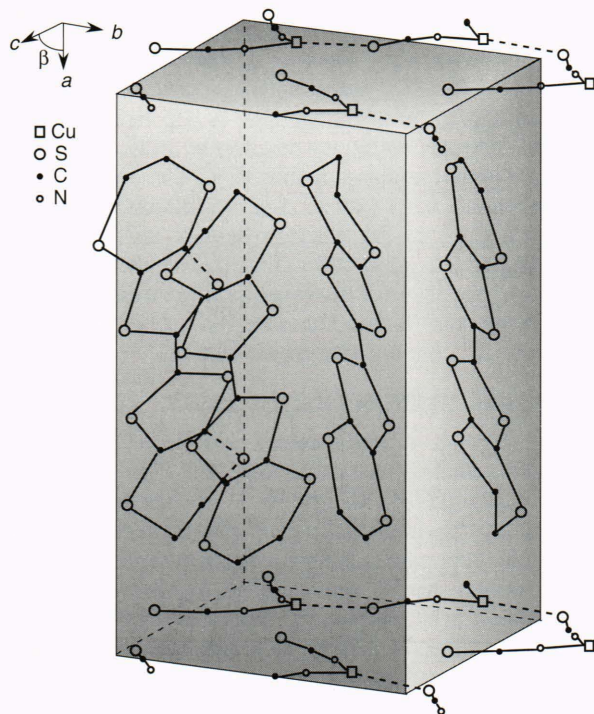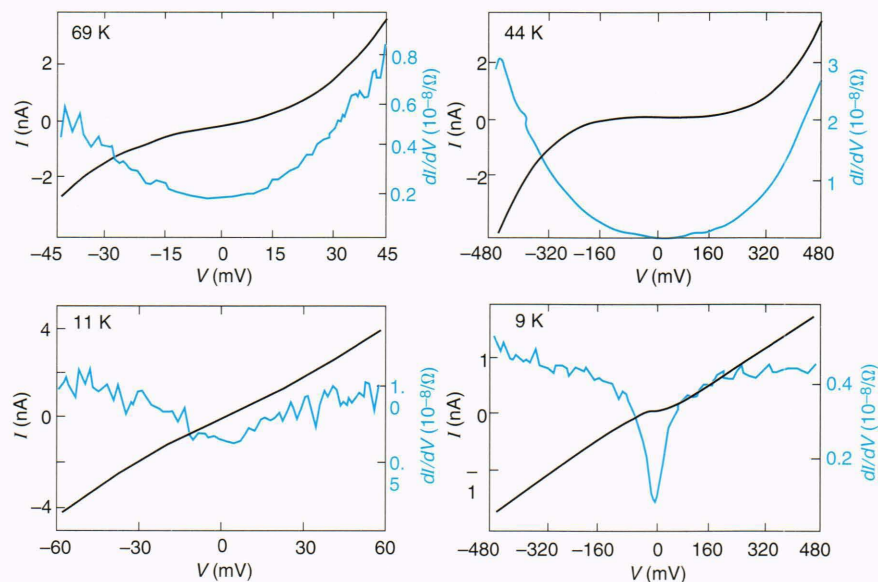

Figure 7. Crystal structure of κ-$[(BEDT\text{-}TTF)_2]^+[Cu(NCS)_2]^-$.

Table 1. Crystallographic data of κ-$[(BEDT\text{-}TTF)_2]^+[Cu(NCS)_2]^-$ (from Ref. 31).

Temp. (K)	a (Å)	b (Å)	c (Å)	β (deg)	V (Å^3)
298	16.248	8.440	13.124	110.30	1688.0
104	16.382	8.402	12.833	111.33	1645.3

tance decreases as the temperature is decreased from room temperature to 240 K. From 240 to 90 K, the material displays a temperature-activated behavior that peaks around 90 K. From 90 K to the superconducting transition that begins at 10.8 K, the material displays metallic behavior (decrease of resistance with temperature). The existence of an activated regime in the normal (nonsuperconducting) region of the resistance versus temperature diagram is a peculiar and yet not fully understood behavior of all the κ-phased ET compounds. In $[(ET)_2]^+[Cu(NCS)_2]^-$, this behavior occurs from 240 to 90 K, and a peak in the electrical resistance versus temperature diagram occurs at $\approx$90 K (Fig. 8).

The STM images and spectroscopy of κ-$[(ET)_2]^+$ $[Cu(NCS)_2]^-$ were taken in air at room temperature. The experimental details of the STM operation were similar to those reported in the previous section. The crystals were mounted on gold films evaporated on cleaved mica substrates at 200°C and fixed to the substrates with conductive silver paint. The images were collected with the STM operated in constant current mode and in constant height mode. No apparent differences in the images were observed in the two modes of operation. The tunneling current was set to a value of 1 nA. Scans were made with positive and negative tip bias voltages. The images presented were collected with tip voltages within a ±200-mV range. Tunneling resistances were kept at or above $10^7 \Omega$. The top flat phase of the flake-shaped crystals was

are summarized in Table 1. Note changes in the lattice parameters as the material is cooled.

Four-probe DC conductivity measurements on the κ-$[(ET)_2]^+[Cu(NCS)_2]^-$ samples from room down to liquid helium temperature were made by Syaulan S. Yang, a graduate student also working in Cowan's group at The Johns Hopkins University. The experimental details of the measurement have been reported elsewhere.[33] The temperature dependence of the electrical resistance of κ-$[(ET)_2]^+[Cu(NCS)_2]^-$ is shown in Figure 8. The resis-
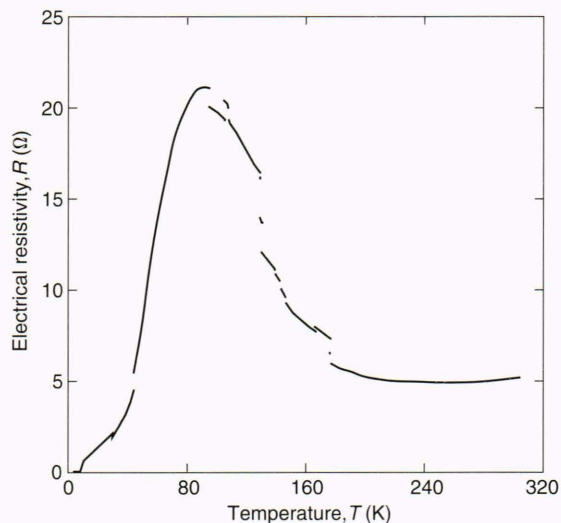
338

Figure 8. Electrical resistance of κ-[(BEDT-TTF)$_2$]$^+$[Cu(NCS)$_2$]$^-$ as a function of temperature.

imaged in all cases. The STM scans ranged in size from 30 Å by 30 Å to 700 Å by 700 Å.

Figures 9A and 9B correspond, respectively, to 67 Å by 67 Å and 70 Å by 70 Å STM images of the bc plane of κ-[(ET)$_2$]$^+$[Cu(NCS)$_2$]$^-$. The images are superimposed with drawings that correspond to the cation (Fig. 9A) and anion (Fig. 9B) unit cells. Since the tunneling current is extremely distance-dependent, only the atoms closer to the probed surface will have a significant contribution to the image; therefore, only the extreme rings of the ET molecule closer to the bc plane will contribute to the cation images (Fig. 9A). Models of the cation and anion structure were superimposed on the images. The models were first scaled to the dimensions of the image, then translated and rotated to provide the best match. The shape and distances within the unit cell of the models are preserved. For the cation (Fig. 9A), for the reasons just explained, only the projection of the two outer rings of the structure of the ET molecule closer to the bc plane was used in the model (Fig. 7). The resolution obtained in Figure 9A is good only for showing the position of the ET molecules within the surface. The unit cell of the models is repeated 3×3 times in both cases, and the agreement with the underlying images in either instance

is excellent. The experimental conditions used to obtain each image are summarized in the figure captions. In Figure 9B, the center of the Y-shaped repeated structure corresponds to the position of the copper atom connected on one end to the sulfur of the preceding unit and to two NCS atom sequences at the Y branches (the intersecting position of the Y branches in two consecutive polymer chain units) (cf. Fig. 7). Note the different intensities in the STM image of consecutive Cu–S bonds within a chain. The difference in intensity defines an additional modulation in the structure commensurate to the lattice with b and c periodicity.

Although several groups have reported STM images[34-37] of κ-[(ET)$_2$]$^+$[Cu(NCS)$_2$]$^-$, most of them show images of the ET cations along the bc plane, as in Figure 9A. High-resolution images of the anions (Fig. 9B) were made at APL for the first time in January 1991. The imaging of the different ions that form the material (Figs. 9A or 9B) does not depend on the STM parameters for tunneling bias voltages within ±200 mV; it depends on the sample conditions. The appearance of one or the other element in the image (Fig. 9A or Fig. 9B) is related to the way the crystal terminates rather than to the tunneling conditions (tunneling current or bias voltage settings) or the different modes of operating the STM (constant current or constant height). This relationship means that images revealing the cation structure were taken on a crystal in which the ET molecules formed the last layer, and, similarly, images revealing the anion structure were taken on a crystal in which the Cu(NCS)$_2$ polymeric chains formed the last layer. Both crystals were synthesized in the same batch.

The STM images demonstrate definitively the lack of disorder and structural irregularities present in the crystal structure as proposed by other groups.[26-28] The STM images of the anions in κ-[ET]$^+$[Cu(NCS)$_2$]$^-$ provide direct evidence of an additional periodicity in the spatial dependence of the electron density of states. The existence of this modulation is surprising because even though the environment of both copper atoms that appear in the unit cell is the same (equivalent positions), only one of the two S–Cu bonds in the unit cell appears highlighted in the STM images. The nature of the modulation is currently unknown; other experimental results that may suggest a possible interpretation are being examined.
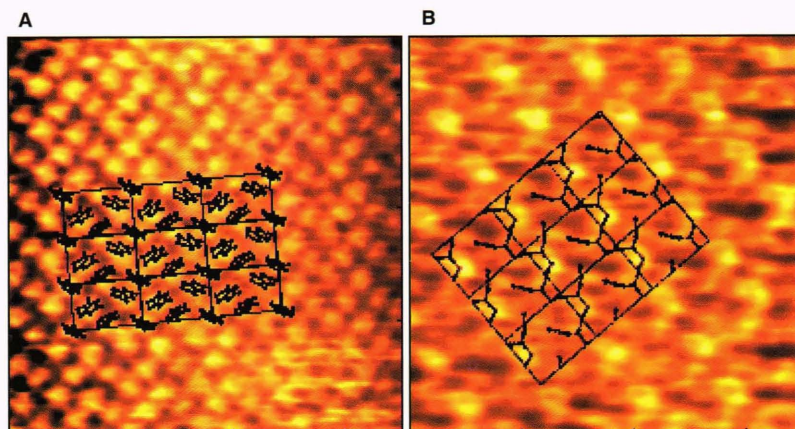

Figure 9. Scanning tunneling microscope images of the bc plane of κ-[(BEDT-TTF)$_2$]$^+$[Cu(NCS)$_2$]$^-$ in air at room temperature. **A.** 67 Å by 67 Å scan. **B.** 70 Å by 70 Å scan. In A, the model of molecular structure of the outer ring of the BEDT-TTF cations is projected onto the bc plane. ($V_{tip} = -200$ mV, $I_{tun} = 1$ nA, constant height mode). In B, the model of the molecular structure of the anions is projected onto the bc plane. ($V_{tip} = 50$ mV, $I_{tun} = 1$ nA, constant current mode). From Ref. 46, copyright 1992 by the AAAS.

Different studies of κ-[ET]$^+$[Cu(NCS)$_2$]$^-$ have suggested the presence of a CDW in the material on the basis of observed anisotropy of the electrical conductivity in the *bc* plane of the material and on magnetoresistance measurements that help determine the Fermi surface. These results suggest the existence of nested states in the Fermi surface (nesting occurs when regions of the Fermi surface overlap when the surface is translated by a vector **q**; for the CDW, q = 2 k_F) and hence the presence of a CDW (the origin of the charge density instability is the presence of nested states; in one-dimensional materials, the nesting is perfect).[38] The only structural evidence for an anisotropy of the *bc*-plane conductivity may come from the anions, because the ET molecules in that projection form a nearly perfect two-dimensional network. The polymeric chains formed by the anions, on the other hand, provide a one-dimensional character to the structure and may indeed be responsible for the in-plane anisotropy. X-ray absorption fine-structure results[39] suggest that the anions have an important role in the normal conductivity of the material. This finding is manifested in the STM images, because the anions contribute to the density of states near the Fermi level and are therefore resolved by the STM. If the anions were simply insulating spacers between the ET conduction planes, they would not contribute to the density of states near the Fermi level, and the images would be the result of fluctuations in the tunneling barrier height. Since the anion images reflect height corrugations on the order of 1 Å, barrier height fluctuations of $\approx$1 eV or higher are implied (depending on the tip-to-sample distance) over the Cu(NCS)$_2$ atomic distances.

The existence of a CDW in the material would not be consistent with a modulation that has the same period as the undistorted lattice. We speculate that if the additional modulation present in the anion images is due to the presence of a CDW commensurate with the lattice as observed in TTF-TCNQ and other low-dimensional organic systems, then an additional modulation (with longer period) that the current images do not resolve should be present. The presence of a CDW in the material with an incommensurate-to-commensurate transition at 240 K would explain the opening of a gap in the electron density of states near the Fermi level and the transition in the resistance from a metallic to a temperature-activated regime, as shown in Figure 8. As the temperature decreases, the material goes through a pronounced contraction in the *c* direction and an expansion in the *a* direction (as seen in Table 1). In particular, the *c* direction contraction would bring the polymeric chains closer together, thereby increasing the interchain interaction and diminishing the one-dimensional character of the material. This result would cause the projection of the Fermi surface along the *bc* plane to become more circular, the nested states and the CDW to disappear, the gap to close, and the material to become metallic. This model is consistent with other experimental results that show the suppression of the anomalous resistance behavior by the application of external pressure[40,41] and the enhancement of the behavior by the application of tension along the *b* direction.[42]

CONCLUSIONS

This article summarizes the results of previous studies made in TTF-TCNQ and related compounds and in κ-[(ET)$_2$]$^+$[Cu(NCS)$_2$]$^-$.[33,43-46] The STM has been successfully used to study the structure and the electron density of states of organic conductors and superconductors, and the effects of low dimensionality in the electron density of states of these materials. Alternative experiments for detecting CDW's using diffraction are less direct and very difficult to perform. The STM in a direct way can reveal the presence of electron density distortions that have a strong effect on the electrical behavior of the materials. By revealing and understanding the mechanisms that either affect or prevent high-temperature superconductivity in organic materials, we may be able to engineer molecules and materials that will provide us with the properties we desire.

REFERENCES

[1] Binning, G., Rohrer, H., Gerber, C., and, Weibel, E., "Surface Studies by Scanning Tunneling Microscopy," *Phys. Rev. Lett.* **49**, 57 (1982).

[2] Hess, H. F., Robinson, R. B., Dynes, R. C., Valles, J. M., Jr., and Waszczak, J. V., "Scanning-Tunneling-Microscope Observation of the Abrikosov Flux Lattice and the Density of States Near and Inside a Fluxoid," *Phys. Rev. Lett.* **62**, 214 (1989).

[3] Coleman, R. V., Gimbattista, B., Hansma, P. K., Johnson, A., McNairy, W. W., et al., "Scanning Tunneling Microscopy of Charge-Density Waves in Transition Metal Chalcogenides," *Adv. Phys.* **37**, 559 (1988).

[4] Eigler, D. M., and Schweizer, E. K., "Positioning Single Atoms with a Scanning Tunnelling Microscope," *Nature* **344**, 524 (1990).

[5] Eigler, D. M., and Schweizer, E. K., "An Atomic Switch Realized with the Scanning Tunnelling Microscope," *Nature* **352**, 600 (1991).

[6] Little, W. A., "Possibility of Synthesizing an Organic Superconductor," *Phys. Rev.* **134A**, 1416 (1964).

[7] Peierls, R. E., *Quantum Theory of Solids,* Oxford University Press, p. 111 (1954).

[8] Fröhlich, H., *Proc. R. Soc. London Ser. A* **223**, 296 (1954).

[9] Jérome, D., Mazaud, A., Ribault, M., and Bechgaard, K., "Superconductivity in a Synthetic Organic Conductor (TMTSF)$_2$PF$_6$," *J. Phys. (Paris) Lett.* **41**, L95 (1980).

[10] Urayama, H., Yamochi, H., Saito, G., Nozawa, K., Sugano, T., et al., "A New Ambient Pressure Organic Superconductor Based on BEDT-TTF with T$_c$ Higher than 10K (T$_c$ = 10.4K)," *Chem. Lett.* **1988**, 55 (1988).

[11] Williams, J. M., Schultz, A. J., Geiser, U., Carlson, K. D., Kini, A. M., et al., "Organic Superconductors–New Benchmarks," *Science* **252**, 1501 (1991).

[12] Tersoff, J., and Hamann, D. R., "Theory and Application for the Scanning Tunneling Microscope," *Phys. Rev. Lett.* **50**, 1998 (1983).

[13] Tersoff, J., and Hamann, D. R., "Theory of the Scanning Tunneling Microscope," *Phys. Rev.* **B31**, 805 (1985).

[14] Hansma, P., and Tersoff, J., "Scanning Tunneling Microscopy," *J. Appl. Phys.* **61**, R1 (1987).

[15] Bardeen, J., "Tunnelling from a Many-Particle Point of View," *Phys. Rev. Lett.* **6**, 57 (1961).

[16] Kuk, Y., and Silverman, P. J., "Scanning Tunneling Microscope Instrumentation," *Rev. Sci. Instrum.* **60**, 165 (1989).

[17] Kaplan, M. L., "A Three-Chamber Diffusion Apparatus for the Growth of Single Crystals of Organic Donor–Acceptor Salts," *J. Cryst. Growth* **33**, 161 (1976).

[18] Kistenmacher, T. J., Phillips, T. E., and Cowan, D. O., "The Crystal Structure of the 1:1 Radical Cation–Radical Anion Salt of 2,2'-Bis-1,3-dithiole (TTF) 7,7,8,8-Tetracyanoquinodimethane (TCNQ)," *Acta Crystallogr.* **B30**, 763 (1974).

[19] Jerome, D., and Schulz, H. J., "Organic Conductors and Superconductors," *Adv. Phys.* **31**, 359 (1982).

[20] Sleator, T., and Tycko, R., "Observation of Individual Molecules at a Crystal Surface with Use of a Scanning Tunneling Microscope," *Phys. Rev. Lett.* **60**, 1418 (1988).

[21] Fainchtein, R., and Zarriello, P. R., "A Computer-Controlled Technique for Electrochemical STM Tip Fabrication" (patent pending), *J. Ultramicroscopy* (in press).

[22] Kagoshima, S., Anzai, H., Kajimura, K., and Ishiguro, T., "Observation of the Kohn Anomaly and the Peierls Transition in TTF-TCNQ by X-Ray Scattering," *J. Phys. Soc. Jpn.* **39**, 1143 (1975).

[23] Kagoshima, S., Ishiguro, T., and Anzai, H., "X-Ray Scattering Study of Phonon Anomalies and Superstructures in TTF-TCNQ," *J. Phys. Soc. Jpn.* **41**, 2061 (1976).

[24] Denoyer, F., Comes, F., Garito, A. F., and Heeger, A. J., "X-Ray Diffuse-Scattering Evidence for a Phase Transition in Tetrathiafulvalene Tetracyanoquinodimethane (TTF-TCNQ)," *Phys. Rev. Lett.* **37**, 445 (1975).

[25] Pouget, J. P., Khanna, S. K., Denoyer, F., and Comes, R., "X-Ray Observation of $2k_F$ and $4k_F$ Scattering in Tetrathiafulvalene-Tetracyanoquinodimethane (TTF-TCNQ)," *Phys. Rev. Lett.* **37**, 437 (1976).

[26] Khanna, S. K., Pouget, J. P., Comes, R., Garito, A. F., and Heeger, A. J., "X-Ray Studies of $2k_F$ and $4k_F$ Anomalies in Tetrathiafulvalene-Tetracyanoquinodimethane (TTF-TCNQ)," *Phys. Rev. B* **16**, 1468 (1976).

[27] Comes, R., Shapiro, S. M., Shirane, G., Garito, A. F., and Heeger, A. J., "Neutron Scattering Study of the 38- and 54-K Phase Transitions in Deuterated Tetrathiafulvalene-Tetracyanoquinodimethane (TTF-TCNQ)," *Phys. Rev. Lett.* **35**, 1518 (1975).

[28] Kagoshima, S., Nagasawa, H., and Sambongi, T., *One-Dimensional Conductors*, Springer-Verlag, Berlin, Heidelberg, pp. 67–82 (1987).

[29] Leo, V., "Elastic Electron Tunneling Study of the Metal-Insulator Transition in TTF-TCNQ," *Solid State Commun.* **40**, 509 (1981).

[30] Etemad, S., "Systematic Study of the Transitions in Tetrathiafulvalene-Tetracyanoquinodimethane (TTF-TCNQ) and its Selenium Analogs," *Phys. Rev.* **B13**, 2254 (1976).

[31] Urayama, H., Yamochi, H., Saito, G., Sato, S., Kawamoto, A., et al., "Crystal Structures of Organic Superconductor, $(BEDT\text{-}TTF)_2Cu(NCS)_2$, at 298 K and 104 K," *Chem. Lett.* **1988**, 463 (1988).

[32] Ravy, S., Pouget, J. P., Lenoir, C., and Batail, P., "Short Range Modulation in the Organic Superconductor $(BEDT\text{-}TTF)_2Cu(NCS)_2$," *Solid State Commun.* **73**, 37 (1990).

[33] Fainchtein, R., D'Arcangelis, S. T., Yang S. S., and Cowan, D. O., "Study of the Solid State Properties of an Organic Superconductor," in *Proc. Fall Meeting of the Materials Research Society, Symp. Electrical, Optical and Magnetic Properties of Organic Solid State Materials*, Boston, 2–6 Dec 1991, Materials Research Society, N.Y. (in press).

[34] Yoshimura, M., Shigekawa, H., Nejoh, H., Saito, G., Saito, Y., et al., "Electronic Structure of the Organic Superconductor $\kappa\text{-}(BEDT\text{-}TTF)_2Cu(NCS)_2$ [where BEDT-TTF is bis(ethylenediothio)terathiafulvalene] Studied by Scanning Tunneling Microscopy," *Phys. Rev. B* **43**, 13,590 (1991).

[35] Miura, Y. F., Kasai, A., Nakamura, T., Komizu, H., Matsumoto, M., et al., "Scanning Tunneling Microscopy Study of $\kappa\text{-}(BEDT\text{-}TTF)_2Cu(NCS)_2$ and $\alpha\text{-}(BEDT\text{-}TTF)_2I_3$," *Mol. Cryst. Liq. Cryst.* **196**, 161 (1991).

[36] Mori, Y., Maruyama, J., Mori, H., and Saito, G., "Electronic Structure of $(BEDT\text{-}TTF)_2X$ Salts Studied by Scanning Tunneling Spectroscopy," *Japn. J. Appl. Phys.* **30**, L358 (1991).

[37] Magonov, S. N., Bar, G., Keller, E., Yagubskii, E. B., and Laukhina, E. E., "Surface Analysis of Organic Superconductors by Scanning Probe Techniques–STM and AFM," *Ultramicroscopy* (in press).

[38] Wolf, S. A., and Kresin V. Z., "Organics vs Cuprates: Why is T_c Still so Low in the Organics," in *Organic Superconductivity*, Kresin, V. Z., and Little, W. A. (eds.), Plenum Press, N.Y., p. 31 (1990).

[39] Doi, T., Oshima, K., Yamazaki, H., Maruyama, H., Maeda, H., et al., "Anomalous Temperature-Dependent Local Structure in $\kappa\text{-}(BEDT\text{-}TTF)_2Cu(NCS)_2$," *J. Phys. Soc. Jpn.* **60**, 1441 (1991).

[40] Parker, I. D., Friend, R. H., Kurmoo, M., Day, P., Lenoir, C., et al., "Pressure Dependence of the Transport Properties of the Molecular Superconductor, $\kappa\text{-}(BEDT\text{-}TTF)_2Cu(NCS)_2$," *J. Phys.: Condens. Matter* **1**, 4479 (1989).

[41] Toyota, N., and Sasaki, T., "On the Resistance Maximum in High-T_c-κ-$(BEDT\text{-}TTF)_2Cu(NCS)_2$," *Solid State Commun.* **74**, 361 (1990).

[42] Kusuhara, H., Sakata, Y., Ueba, Y., Tada, K., Kaji, M., et al., "Tensile Stress Effect on Transport Properties of $(BEDT\text{-}TTF)_2Cu(NCS)_2$," *Solid State Commun.* **74**, 251 (1990).

[43] Fainchtein, R., Pan S., and de Lozanne, A. L., "Scanning Tunneling Microscopy and Spectroscopy of Quasi One-Dimensional Organic Conductors," in *Organic Superconductivity*, Kresin, V. Z., and Little, W. A. (eds.), Plenum Publishing Corp., p. 147 (1990).

[44] Pan, S., de Lozanne, A. L., and Fainchtein, R., "Scanning Tunneling Microscopy of Quasi-One-Dimensional Organic Conductors," *J. Vac. Sci. Technol.* **B9**, 1017 (1991).

[45] Fainchtein, R., "Effects of Low Dimensionality in the Electrical Conductivity of Organic Superconductors", in *Proc. XIII Winter Meeting on Low Temperature Physics*, Morelos, Mexico (in press).

[46] Fainchtein, R., D'Arcangelis, S. T., Yang, S. S., and Cowan, D. O., "Evidence of Order and Low Dimensionality in the Organic Superconductor $(BEDT\text{-}TTF)_2Cu(NCS)_2$ Revealed by STM," *Science* **256**, 1012–1014 (1992).

[47] Grüner, G. , "The Dynamics of Charge Density Waves," *Rev. Mod. Phys.* **60**,

THE AUTHOR

RAÚL FAINCHTEIN is a senior staff physicist in the Research Center's Materials Characterization Group. Born in Mexico, he obtained a B.S. degree in physics from the Instituto Tecnologico y de Estudios Superiores de Monterrey in 1977 and a Ph.D. degree in physics from The University of Texas at Austin in 1983. From 1983 to 1987, he completed two postdoctoral fellowships, the first at The University of Texas at Austin and the second at The Pennsylvania State University. After joining APL in 1987, he began work in scanning tunneling microscopy. His interests include characterization of the structure and properties of materials, quasi-one-dimensional systems, organic conductors, superconductors, thin films, and noncrystalline materials. Dr. Fainchtein's expertise is in the areas of tunneling microscopy and other scanning surface probes, neutron scattering, optical spectroscopy, and Raman scattering.